Identification and elimination of inductively coupled plasma-induced defects in $Al_xGa_{1-x}N$/GaN heterostructures*

Lin Fang(林 芳)[a], Shen Bo(沈 波)[a]†, Lu Li-Wu(卢励吾)[a], Liu Xin-Yu(刘新宇)[b], Wei Ke(魏 珂)[b], Xu Fu-Jun(许福军)[a], Wang Yan(王 彦)[a], Ma Nan(马 楠)[a], and Huang Jun(黄 俊)[b]

[a] *State Key Laboratory of Artificial Microstructures and Mesoscopic Physics, School of Physics, Peking University, Beijing* 100871, *China*

[b] *Institute of Microelectronics, Chinese Academy of Sciences, Beijing* 100029, *China*

(Received 30 November 2010; revised manuscript received 25 March 2011)

By using temperature-dependent Hall, variable-frequency capacitance–voltage and cathodoluminescence (CL) measurements, the identification of inductively coupled plasma (ICP)-induced defect states around the $Al_xGa_{1-x}N$/GaN heterointerface and their elimination by subsequent annealing in $Al_xGa_{1-x}N$/GaN heterostructures are systematically investigated. The energy levels of interface states with activation energies in a range from 0.211 to 0.253 eV below the conduction band of GaN are observed. The interface state density after the ICP-etching process is as high as 2.75×10^{12} $cm^{-2}\cdot eV^{-1}$. The ICP-induced interface states could be reduced by two orders of magnitude by subsequent annealing in N_2 ambient. The CL studies indicate that the ICP-induced defects should be Ga-vacancy related.

Keywords: inductively coupled plasma, subsequent annealing, defect state

PACS: 73.40.Qv, 73.20.Hb, 73.20.At, 73.50.Dn **DOI:** 10.1088/1674-1056/20/7/077303

1. Introduction

Because of the inherent chemical stability of GaN, the device fabrication process involving a GaN-based material system usually relies on dry etching, which is known to cause surface damage.[1] In particular, the surface damage induced in a recessed gate process in the fabrication of $Al_xGa_{1-x}N$/GaN heterostructure field effect transistors (HFETs) can drastically lower the Schottky barrier heights of the gate metals and reduce the gate breakdown voltage unless a very low plasma power is used.[2–4] Dry etching-induced damage is attributed to the formation of a nonstoichiometric surface due to preferential loss of one of the elements.[5] Another possible origin of the degradation is the generation of trapping centres on the etched surface. A number of research efforts have been made to identify and eliminate the dry etching-induced damage on n-type GaN.[6,7] In deep-level transient spectroscopic (DLTS) measurements on n-type GaN, the shallow levels with activation energies ranging from 0.18 to 0.22 eV are commonly observed and suggested to be related to the N vacancy (V_N). However, little work has been done on the elimination of dry etching-induced damage in $Al_xGa_{1-x}N$/GaN heterostructures.

There is no well-known and tested procedure for the analysis of the variable-frequency capacitance–voltage (C–V) method from a metal/insulator/$Al_xGa_{1-x}N$/GaN (MIS) structure to extract the interface state densities and the interface state energy levels at the insulator/$Al_xGa_{1-x}N$ and the $Al_xGa_{1-x}N$/GaN interfaces. For Si_3N_4-passivated $Al_xGa_{1-x}N$/GaN heterostructures, the related DLTS results showed a remarkable decrease in state density at the Si_3N_4/$Al_xGa_{1-x}N$ interface (ranging from 1×10^{11} to 5×10^{11} $cm^{-2}\cdot eV^{-1}$).[8,9] In this work, we focus on the identification of inductively coupled plasma (ICP) induced interface states around the $Al_xGa_{1-x}N$/GaN interface and their elimination by subsequently annealing the $Al_xGa_{1-x}N$/GaN MIS structure samples.

2. Experiments

The $Al_{0.25}Ga_{0.75}N$/GaN heterostructures were grown on the (0001) surface of sapphire sub-

*Project supported by the National Natural Science Foundation of China (Grant Nos. 60906041, 10774001, 60736033, and 60890193) and the National Basic Research Program of China (Grant Nos. 2006CB604908 and 2006CB921607).

†Corresponding author. E-mail: bshen@pku.edu.cn

© 2011 Chinese Physical Society and IOP Publishing Ltd

strate using metal-organic chemical vapour deposition (MOCVD). A nucleation GaN buffer layer was grown at 530 °C followed by a 2.2-μm-thick unintentionally doped GaN (i-GaN) layer deposited at 1070 °C. The temperature was then increased to 1090 °C to grow an approximately 1-nm-thick AlN interlayer and a 25-nm-thick unintentionally doped $Al_{0.25}Ga_{0.75}N$ barrier. The room temperature (RT) Hall mobility and density of the two-dimensional electron gas (2DEG) in the heterostructures were 1490 $cm^2/V{\cdot}s$ and 9.350×10^{12} cm^{-2}, respectively.

After the MOCVD growth, samples with van der Pauw configurations and MIS structures were fabricated. Ti/Al/Ti/Au (20/180/55/45 nm) Ohmic contacts was deposited in sequence using an electron beam evaporator, followed by rapid thermal annealing in a N_2 ambient at 850 °C for 30 s. Afterwards, the ICP etching and subsequent annealing were performed on the samples. The surfaces of the $Al_{0.25}Ga_{0.75}N$/GaN heterostructures were etched using ICP with a mixture of Cl_2 (10 sccm) and BCl_3 (2 sccm) at the inductive power of 180 W and the rf chuck power of 2 W for 20 s. The etching depth for each sample was 5–6 nm, which is an accurate and repeatable value for the gate recess process. After ICP etching, the samples were annealed in a N_2 ambient at 350 °C, 650 °C and 850 °C for 30 s, separately. Five sets of samples were prepared. For reference, the first set was without ICP etching and subsequent annealing (as-prepared); after ICP etching, the second set did not undergo subsequent annealing (as-etched); the three other sets were annealed at 350 °C (ICP350), 650 °C (ICP650) and 850 °C (ICP850), separately. The Si_3N_4 (100-nm-thick) insulating layer was deposited by plasma-enhanced CVD on the surface of the $Al_xGa_{1-x}N$ barrier layer. Finally, the Ni/Au (40/150 nm) electrode was evaporated on the top of the Si_3N_4 insulating layer.

The temperature-dependent Hall measurements were performed on an Accent HL5500 Hall measurement system with an HL5550 liquid N_2 stage in vacuum and a temperature ranging from 90 to 450 K. An Agilent 4155C semiconductor parameter analyzer and an Agilent 4294A precision impedance analyzer with a 100 mV test signal were used for current–voltage (I–V) and C–V measurements, respectively. The cathodoluminescence (CL) spectra wave investigated at RT with an electron beam accelerating voltage of 2 kV in a scanning electron microscope (SEM) equipped with an Oxford Mono-CL3.

3. Results and discussion

Figures 1(a) and 1(b) show the temperature dependences of the mobility and density of the 2DEG in $Al_{0.25}Ga_{0.75}N$/GaN heterostructures for as-prepared, as-etched, ICP350, ICP650 and ICP850 samples, respectively. The 2DEG mobility decreases with the increase of temperature, indicating that the 2DEG mobility is limited primarily by ionized impurities scattering at lower temperatures and longitudinal optical phonon scattering at higher temperatures.[10,11] The 2DEG density remains almost unchanged with the temperature increasing from 90 to 300 K and begins to decrease with the temperature increasing above 300 K. It is believed that the decrease of the $Al_{0.25}Ga_{0.75}N$/GaN heterostructure conduction band offset accounts for the decrease of the 2DEG density as the temperature increases[12] From Fig. 1, we can also see that both the mobility and the density of the 2DEG decrease remarkably after the ICP etching process, and then gradually climb back to the as-prepared sample level after the subsequent annealing.

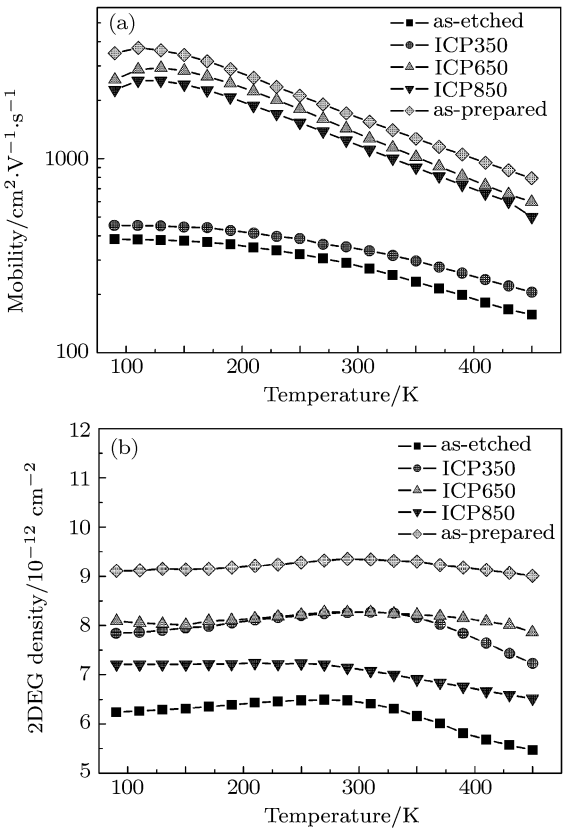


Fig. 1. Temperature dependences of (a) mobility and (b) density of 2DEG in $Al_{0.25}Ga_{0.75}N$/GaN heterostructures for as-prepared, as-etched, ICP350, ICP650 and ICP850 samples.

There are three main reasons for the change of the 2DEG density: 1) ICP etching-induced crystal lattice

damage weakens the polarization in the $Al_xGa_{1-x}N$ layer, which leads to a decrease in the 2DEG density, and the annealing-induced recovery of the crystal lattice damage promotes the increase of the 2DEG density; 2) considering the surface donor model, the 2DEG density decreases with the thinning of the $Al_xGa_{1-x}N$ barrier due to ICP etching (5–6 nm);[13] 3) ICP etching induces lattice defects which generally behave as deep level states. When the $Al_xGa_{1-x}N$ barrier layer contains ICP induced defects distributed around the Fermi level, some channel electrons will be captured. However, subsequent annealing at higher temperature (ICP850) can cause the defects to congregate around the $Al_xGa_{1-x}N$/GaN heterointerface and make the mobility and density of the 2DEG decrease again.[14]

Figure 2 shows the 100 kHz C–V characteristics for as-etched, ICP350, ICP650 and ICP850 samples at RT. Because the 2DEG densities are different from each other for these samples, the applying negative bias voltage values of the 2DEG complete depletion are different. It is worth noting that an obvious peak located at the negative bias voltage of about −25 V appears for the as-etched sample. This peak corresponds to the ICP-induced defect state. We can also observe that the peaks related to the ICP-induced defect states become less prominent with the increase of the subsequent annealing temperature for ICP350, ICP650 and ICP850 samples. This peak position is around the complete depletion region of the 2DEG, and so the ICP-induced defect states should be located near the $Al_xGa_{1-x}N$/GaN heterointerface. The trapped electrons will sweep out from the metal/Si_3N_4 interface, the Si_3N_4 layer and the Si_3N_4/$Al_xGa_{1-x}N$ interface at this large negative bias voltage, as shown in Fig. 3(b). The fact that the amplitude of the peak lowers obviously with the increase of subsequent annealing temperature indicates a pronounced decrease of the ICP-induced defect states.

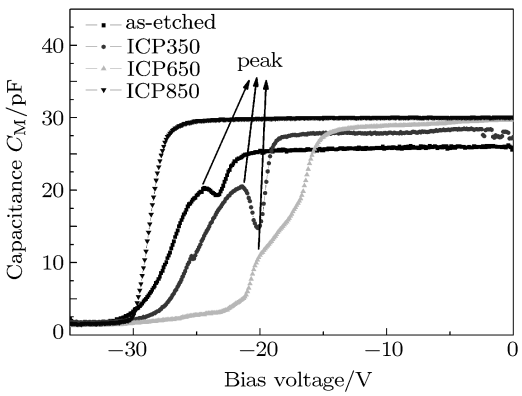


Fig. 2. The 100 kHz C–V characteristics for as-etched, ICP350, ICP650 and ICP850 samples at RT.

Figure 3(a) shows the frequency dependences of the interface state capacitance for as-etched, ICP350, ICP650 and ICP850 samples at RT, with the applied voltage value selected at the corresponding bias voltage where the relevant ICP-etching peak shown in Fig. 2 appears. Figure 3(b) shows the schematic energy-band diagram of the $Al_{0.25}Ga_{0.75}N$/GaN MIS structure at the negative bias voltage. Figure 3(c) shows the equivalent circuit and the simplified equivalent circuit of the $Al_{0.25}Ga_{0.75}N$/GaN MIS structure at the negative bias voltage.

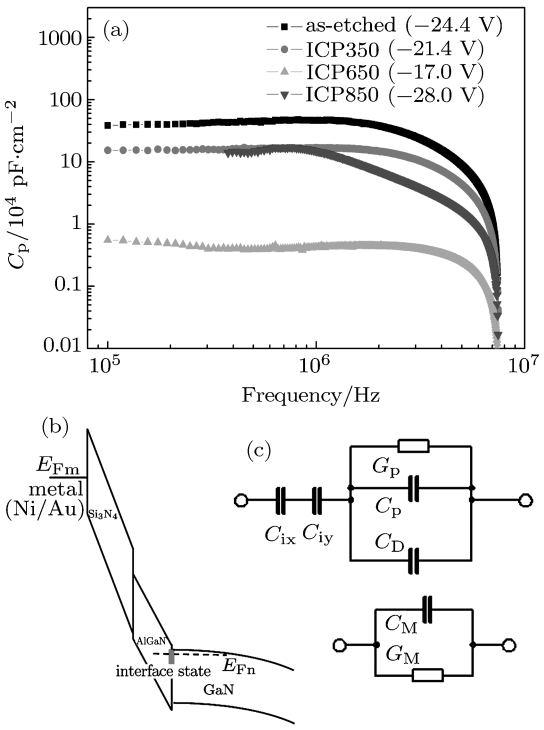


Fig. 3. (a) Frequency dependence of the interface state capacitance with different bias voltages for as-etched, ICP350, ICP650 and ICP850 samples at RT (the applied voltage value is selected at the corresponding bias voltage where the relevant ICP-etching peak appears); (b) the schematic energy-band diagram of $Al_{0.25}Ga_{0.75}N$/GaN MIS structures at negative bias voltage (E_{Fm} is the Femi level of metal and E_{Fn} is the Femi level of GaN); (c) the equivalent circuit and simplified equivalent circuit of $Al_{0.25}Ga_{0.75}N$/GaN MIS structures at negative bias voltage.

Described in the following parts is the measurement method to extract defect state parameters from the variable-frequency C–V characteristics.[15–18] Measurements of the device conductance G_M and the device capacitance C_M each as a function of frequency f ranging from 100 kHz to 7.5 MHz were performed. The full circuit model of $Al_{0.25}Ga_{0.75}N$/GaN MIS structure employed in our analysis is shown in Fig. 3(c), where C_{ix} is the insulating layer capacitance, C_{iy} is the $Al_xGa_{1-x}N$ barrier layer capacitance,

$C_{\rm p}$ is the interface state equivalent capacitance, $G_{\rm p}$ is the interface state equivalent conductance and $C_{\rm D}$ is the depletion region capacitance. The analysis of the interface state density may be performed on the assumption that the interface state is comprised of a continuum of levels. $C_{\rm p}$ and $G_{\rm p}$ are given by

$$C_{\rm p} = C_{\rm p}^0 \frac{\text{arctg}\omega\tau}{\omega\tau}, \tag{1}$$

$$G_{\rm p} = \omega C_{\rm p}^0 \frac{\ln(1+\omega^2\tau^2)}{2\omega\tau}, \tag{2}$$

where

$$C_{\rm p}^0 = q^2 A N_{\rm ss}. \tag{3}$$

Here, ω is the circular frequency of the test signal and τ is the interface state time constant, with q being the electronic charge, A the contact area and $N_{\rm ss}$ the interface state density. We can obtain $C_{\rm p}$ from the measured device capacitance $C_{\rm M}$ by

$$C_{\rm p} = C_{\rm i}\left(\frac{1}{\dfrac{C_{\rm i}}{C_{\rm M}}-1} - \frac{1}{\dfrac{C_{\rm i}}{C_{\rm M,HF}}-1}\right), \tag{4}$$

where

$$1/C_{\rm i} = 1/C_{\rm ix} + 1/C_{\rm iy}, \tag{5}$$

where $C_{\rm M,HF}$ is the high-frequency capacitance. The interface state capture cross section $\sigma_{\rm n}$ is given by

$$\sigma_{\rm n} = (\tau v_{\rm th} N_{\rm D})^{-1} \exp(-qV_{\rm s}/kT), \tag{6}$$

where $v_{\rm th}$ is the thermal velocity of electrons, $N_{\rm D}$ is the ionized impurity concentration, $V_{\rm s}$ is the semiconductor surface potential, k is Boltzmann's constant and T is the absolute temperature. The interface state energy level is given by

$$E_{\rm c} - E_{\rm T} = q(V_{\rm S} + V_{\rm B}), \tag{7}$$

where $V_{\rm B}$ is the potential difference between the conduction-band edge and the Fermi level. We obtain $qV_{\rm B} = 0.03$ eV from the temperature-dependent Hall measurements. By plotting $C_{\rm p}$ and $G_{\rm p}$ each as a function of frequency and fitting the resulting curves to Eqs. (1) and (2), the interface state density $N_{\rm ss}$ and the interface state time constant τ may be extracted. Based on the work of Nakamura *et al.*,[19] $\sigma_{\rm n}$ is given to be 5.8×10^{-15} cm^2. We obtain the semiconductor surface potential $V_{\rm s}$ from Eq. (6) and the interface state energy level from Eq. (7). Here, the analysis of capacitance–frequency (C–f) characteristics cannot strictly describe an interface effect. It can be best described as the overall effect including the real interface states at the $Al_xGa_{1-x}N$/GaN interface and the trap states inside the $Al_xGa_{1-x}N$ barrier layer and the GaN layer which are close to the $Al_xGa_{1-x}N$/GaN heterointerface (near-interface states). Table 1 shows the simulation results of the defect states located around the $Al_xGa_{1-x}N$/GaN heterointerface for as-etched, ICP350, ICP650 and ICP850 samples.

Table 1. Simulation results of the interface state density $N_{\rm ss}$, the interface state time constant τ and the interface state energy level $E_{\rm C} - E_{\rm T}$ for as-etched, ICP350, ICP650 and ICP850 samples.

	$N_{\rm ss}/10^{12}$ cm^{-2}·eV^{-1}	$\tau/10^{-7}$ s	$E_{\rm C} - E_{\rm T}$/eV
as-etched	2.75	1.75	0.237
ICP350	1.04	1.43	0.232
ICP650	0.028	0.637	0.211
ICP850	1.07	3.18	0.253

According to the variable–frequency C–V analysis, interface state energy levels with the activation energies in a range between 0.211 and 0.253 eV are obtained, and the interface state density after ICP-etching has reached as high as 2.75×10^{12} cm^{-2} eV^{-1}. After ICP-etching and subsequent annealing, three kinds of interface state densities are obtained and characterized. The ICP-induced interface states could be reduced two orders of magnitude by annealing at 650 °C.

A series of CL spectra was obtained for as-prepared, as-etched, ICP350, ICP650 and ICP850 samples at RT, as shown in Fig. 4. The penetration depth of 2 kV incident electrons into nitride material is about 23 nm, according to Monte Carlo simulations using a single scattering model. The detected CL signals carry the information coming from the regions including the $Al_xGa_{1-x}N$ barrier layer, the $Al_xGa_{1-x}N$/GaN interface and the GaN layer (about 23 nm in depth from the $Al_xGa_{1-x}N$ surface), which are the same as the depletion regions at the negative bias voltage of the complete depletion of the 2DEG in C–V measurements. The CL spectra are normalized to maintain the same integral intensity of the near-band edge (NBE) emissions centred at about 3.4 eV (365 nm) from GaN layer. A sharp peak appears at about 3.8 eV (329 nm) in the CL spectrum, which is ascribed to the $Al_xGa_{1-x}N$ NBE emission. A broad deep-level emission at about 2.23 eV (556 nm) is detected separately from as-etched, ICP350, ICP650 and ICP850 samples, which is ascribed to the yellow luminescence (YL) band of GaN.[20] It is generally attributed to the transition from a shallow donor to a deep acceptor ($V_{\rm Ga}$). It is noted that the intensity of the YL band lowers with the increase of the subsequent annealing temperature. The variation trend of YL intensity is consistent with that of the amplitude of the peak corresponding to ICP-induced defect state.

It indicates that the CL measuring results referring to the YL band should be proof that the ICP-induced defect state is V_{Ga} related.

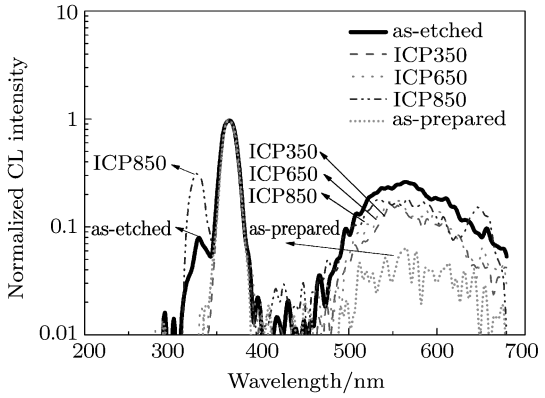


Fig. 4. Typical CL spectra for as-prepared, as-etched, ICP350, ICP650 and ICP850 samples at RT, respectively.

The BCl_3 bombarding plasma is effective in removing native surface oxides on the $Al_xGa_{1-x}N$ surface and enhancing dissociation among Al, Ga and N, and the Cl_2 etching plasma is an effective etcher for the $Al_xGa_{1-x}N$ and GaN layers because of the high volatilities of $AlCl_x$ and $GaCl_x$. So a mixture of Cl_2 and BCl_3 was used to achieve the accurate and repeatable control of etch depth with time.[21] The effective removal of Al and Ga from the $Al_xGa_{1-x}N$ surface appears to be important for the forming of ICP-induced defects.

Trap D, with $E_C - E_T = 0.17 - 0.27$ eV and $\sigma_n = (1-6) \times 10^{-15}$ cm^2, has been observed in thin GaN layers by many groups, using various growth techniques, including hydride vapour phase epitaxy (HVPE),[22,23] MOCVD [24–27] and molecular beam epitaxy (MBE).[28,29] Our experimental results show that the interface state densities within the activation energy range between 0.211 and 0.253 eV are greatly enhanced by the ICP-etching process. Compared with as-etched samples, the ICP350, ICP650 and ICP850 samples show a pronounced decrease in ICP-induced defects, owing to the subsequent annealing. The energy levels in the range between 0.211 and 0.253 eV, as electron traps, might well be related to a defect complex involving V_{Ga} (such as V_N–V_{Ga}), because their activation energies and capture cross sections are very close to those of trap D.[23,24]

4. Conclusion

The identification of ICP-induced defect states around the $Al_xGa_{1-x}N$/GaN heterointerface and their elimination by subsequent annealing in the $Al_xGa_{1-x}N$/GaN heterostructures are systematically investigated by means of temperature-dependent Hall, variable-frequency C–V and CL methods. The interface state levels with the activation energies in a range between 0.211 and 0.253 eV are observed, and the interface state density after the ICP-etching process is as high as 2.75×10^{12} cm^{-2}·eV^{-1}. The ICP-induced defect states can be reduced by two orders of magnitude by subsequent annealing in a N_2 ambient at 650 °C. The CL studies indicate that the ICP-induced defects might be Ga-vacancy related.

References

[1] Adesida I, Youtsey C, Ping A T, Khan F, Romano L T and Bulmann G 1999 *MRS Internet J. Nitride Semicond. Res.* **4S1** G1.4
[2] Chen C H, Keller S, Haberer E D, Zhang L, Denbaars S P, Hy E L and Wu Y 1999 *J. Vac. Sci. Technol.* B **17** 2755
[3] Ping A T, Chen Q, Yang J W, Khan M A and Adesida I 1998 *J. Electron. Mater.* **27** 261
[4] Pearton S, Abermathy C R, Ren F, Lothian J R, Wisk P W and Katz A 1993 *J. Vac. Sci. Technol.* A **11** 1772
[5] Eddy Jr C R and Molnar B 1999 *J. Electron. Mater.* **28** 314
[6] Mouffak Z, Bensaoula A and Trombetta L 2004 *J. Appl. Phys.* **95** 727
[7] Wang X, Yu G, Lei B, Wang X, Lin C, Sui Y, Meng S, Qi M and Li A 2007 *J. Electron. Mater.* **36** 697
[8] Vertiatchikh A V, Eastman L F, Schaff W J and Prunty T 2002 *Electron. Lett.* **38** 388
[9] Hashizume T, Ootomo S, Inagaki T and Hasegawa H 2003 *J. Vac. Sci. Technol.* B **21** 1828
[10] Shah P B, Smith D D, Griffin T E, Jones K A and Sheppard S T 2000 *IEEE Trans. Electron Devices* **47** 308
[11] Maeda N, Tsubaki K, Saitoh T and Kobayashi N 2001 *Appl. Phys. Lett.* **79** 1634
[12] Wang M J, Shen B, Xu F J, Wang Y, Xu J, Huang S, Yang Z J, Xu K and Zhang G Y 2007 *Appl. Phys.* A **88** 715
[13] Smorchkova I P, Elsass C R, Ibbetson J P, Vetury R, Heying B, Fini P, Haus E, DenBaars S P, Speck J S and Mishra U K 1999 *J. Appl. Phys.* **86** 4520
[14] Cai Y, Zhou Y G, Chen K J and Lau K M 2005 *IEEE Electron Device Lett.* **26** 435
[15] Wang R X, Xu S J, Shi S L, Beling C D, Fung S, Zhao D G, Yang H and Tao X M 2006 *Appl. Phys. Lett.* **89** 143505
[16] Miller E J, Dang X Z, Wieder H H, Asbeck P M, Yu E T, Sullivan G J and Redwing J M 2000 *J. Appl. Phys.* **87** 8070
[17] Özdemir A F, Türüt A and Kökçe A 2003 *Thin Solid Films* **425** 210
[18] Lehovec K 1966 *Appl. Phys. Lett.* **8** 48
[19] Nakamura W, Tokuda Y, Ueda H and Kachi T 2006 *Physica* B **376–377** 516
[20] Soh C B, Chua S J, Lim H F, Chi D Z, Tripathy S and Liu W 2004 *J. Appl. Phys.* **96** 1341
[21] Buttari D, Chini A, Palacios T, Coffie R, Shen L, Xing H, Heikman S, McCarthy L, Chakraborty A, Keller S and Mishra U K 2003 *Appl. Phys. Lett.* **83** 4779

[22] Hacke P, Detchprohm T, Hiramatsu K, Sawaki N, Tadatomo K and Miyake K 1994 *J. Appl. Phys.* **76** 304

[23] Fang Z Q, Look D C, Jasinski J, Benamara M, Liliental-Weber Z and Molnar R J 2001 *Appl. Phys. Lett.* **78** 332

[24] Fang Z Q, Look D C, Wang X L, Han J, Khan F A and Adesida I 2003 *Appl. Phys. Lett.* **82** 1562

[25] Fang Z Q, Hemsky J W, Look D C and Mack M P 1998 *Appl. Phys. Lett.* **72** 448

[26] Auret F D, Goodman S A, Koschnick F K, Spaeth J M, Beaumont B and Gibart P 1998 *Appl. Phys. Lett.* **73** 3745

[27] Cho H K, Kim K S, Hong C H and Lee H J 2001 *J. Cryst. Growth* **223** 38

[28] Wang C D, Yu L S, Lau S S, Yu E T, Kim W, Botchkarev A E and Morkoç H 1998 *Appl. Phys. Lett.* **72** 1211

[29] Fang Z Q, Look D C, Kim W, Fan Z, Botchkarev A and Morkoç H 1998 *Appl. Phys. Lett.* **72** 2277